Int. J. Heat Mass Transfer. Vol. 32, No. 4, pp. 735–749, 1989
Printed in Great Britain

0017–9310/89 $3.00 + 0.00

Laboratory studies of thermal convection in the interface under a stable layer

RANGANATHAN KUMAR
Department of Mechanical Engineering, Clemson University, Clemson, SC 29631, U.S.A.

(*Received* 22 *January* 1988 *and in final form* 2 *September* 1988)

Abstract—In a buoyancy-driven penetrative convection experiment, detailed measurements of the local, instantaneous values of temperature, vertical velocity and horizontal velocity are made in the interfacial layer using a thermocouple and a two-component dual beam laser-Doppler velocimeter. In the stable layer internal gravity waves are observed, and the temperature fluctuations in this region are found to oscillate at nearly Brunt–Väisälä frequency. Conditional averaging techniques and probability density distributions are employed to infer the mean properties of the fluid elements in the interfacial layer. The structured regions are named 'coherent' or 'active' and these motions account for 60–70% of the mean square fluctuations in temperature and velocity, and most of the negative heat flux. Interfacial scales are developed and they appear to collapse the data well and keep the scatter in third-order moments within bounds.

1. INTRODUCTION

PENETRATIVE convection occurs in many geophysical flows and it concerns the advance of turbulent flow into a fluid layer of stable stratification. In the lower atmosphere, before sunrise, the air layer is stably stratified. When solar radiation warms the ground, thermals rise penetrating the stable layer after the critical Rayleigh number is exceeded. Some of the warm fluid is entrained downward resulting in mixing of air. In the course of the day, the convective layer increases in thickness at a rate that is determined by the heat flux from the ground. A mixed layer is formed penetrating and entraining the fluid from the stable region. This density jump grows at a much slower rate compared with the growth of an atmospheric inversion. The region that develops between the convection layer and the stable layer has a finite thickness and is called variously the transition zone, interface, interfacial layer or the entrainment zone.

Willis and Deardorff [1] simulated convective entrainment in a water tank experiment. A stably stratified water layer was subjected to an increase in temperature at the lower boundary. Measurements of velocity and temperature fluctuations, and energy fluxes were made. In the interface, large temperature fluctuations were observed and were associated with large positive mean temperature gradients. In their experiment, velocity measurements were made by streak photography of non-buoyant particles. Similar experiments were performed by Heidt [2] who registered temperature profiles, growth rate of inversion and heat fluxes for different temperature profiles. Adrian and Ferreira [3] obtained higher order moments in a non-penetrative convection experiment. Another kind of experiment, turbulent convection in water over ice, was reported by Townsend [4] and Adrian [5]. In this flow, when the lower surface is at 0°C, the bottom layer becomes convectively unstable, capped by a stable gradient above. Adrian [5] presented the higher order moments and discussed the presence of organized structures in the water-over-ice experiment. In another penetrative convection experiment, detailed measurements of all moments including heat flux and joint vertical velocity–temperature moments were made in the interfacial layer for different temperature gradients [6]. The negative heat flux region was well defined in the interface, varying in thickness with different stability gradients.

The power-law dependence of the entrainment velocity of the interface on Richardson number has been the subject of controversy in different geophysical flows in which penetrative convection is important. Kantha *et al.* [7], and Deardorff *et al.* [8] furnished data on the entrainment coefficient that exhibited different power-law dependence of Richardson number (pseudo-Richardson number in the case of windless convection where the convective velocity scale was used). Wyatt [9] analyzed the films from the experiment conducted by Kantha *et al.* [7] to determine relationships between wave and turbulent length and velocity scales. They measured the height of the interface and the standard deviation of the mean height, δ_{int}, called interfacial distortion. Kelvin–Helmholtz type instabilities were observed and their wavelength, amplitude and lifetime were measured. They concluded that at large Richardson number, Ri, the instabilities did not scale with the mixed layer depth, h, whereas at low Ri, $\delta_{\text{int}} \propto h$. In other experiments involving shear, Crapper and Linden [10] and Hopfinger and Toly [11] gave a qualitative picture of the eddies penetrating the interface from the mixed layer.

The inversion rise was well illustrated by several field and aircraft measurements of Lenschow [12], Kaimal *et al.* [13], Caughey and Palmer [14] and Len-

NOMENCLATURE

A	aspect ratio, h/z_*
g	acceleration due to gravity
h	mixed layer depth
Δh	height to which a fluid parcel penetrates
l	length scale of the interface [cm]
N	total area occupied by the fluid
$\dot{N}$	data rate
Q_0	kinematic heat flux at $z = 0$ [°C cm s^{-1}]
Re_*	Reynolds number, $w_* z_*/\nu$
Ri	Richardson number
t	time
t_{BV}	Brunt–Väisälä period
T	mean temperature
ΔT	mean temperature difference
T_∞	mean temperature in the mixed layer
u	horizontal velocity fluctuation
w	vertical velocity fluctuation
$\overline{w\theta}$	kinematic heat flux
w_*	convective velocity scale [cm s^{-1}]
z	vertical coordinate
z_*	mixed layer height
z'	non-dimensional height, $(z - z_*)/l$.

Greek symbols

β	volumetric coefficient of thermal expansion
Γ	constant temperature gradient in the stable layer [°C cm^{-1}]
θ	temperature fluctuation
θ_*	convective temperature scale
θ_c	interfacial temperature scale
ν	kinematic viscosity
σ_u	r.m.s. horizontal velocity
σ_w	r.m.s. temperature fluctuation.

schow *et al.* [15]. Although a complete description of the entrainment zone was given by Caughey and Palmer [14], only the r.m.s. fluctuations of vertical velocity and temperature, and heat flux were obtained, and the atmospheric and field measurements are generally lacking in higher order moments at the interface due to the inherent difficulty in obtaining data in the atmosphere. The normalized third-order moments, $\overline{w^3}$, $\overline{w^2\theta}$, and $\overline{w\theta^2}$, obtained from field measurements [12, 13, 15] were effectively compared in ref. [6] with laboratory measurements. Most of the field data was obtained in the turbulent mixed layer, and hence the moments were normalized by the convective scales.

Substantial progress has been made on the problem of parameterizing the rate of inversion rise and entrainment rate in recent years by Carson [16], Betts [17], Stull [18], Tennekes [19], and Deardorff [20]. Second-order modeling techniques for buoyancy driven mixed layers were presented by Lenschow *et al.* [15] and Zeman and Lumley [21] who utilized gradient transport models for the third-order fluxes that accounted for buoyancy effects. Buoyancy–turbulence interactions couple a flux of one second-order quantity to gradients of other quantities.

The results reported here are an extension of the experiments of ref. [6]. In that paper, attention was focused on a successful simulation of the lower atmosphere, the capability to make LDV measurements in the interface, and the presentation of higher order moments. The r.m.s. temperature fluctuation and turbulent heat flux profiles showed that the data could be collapsed by different length and temperature scales in the entrainment zone. The objectives of the present work are to examine the presence of length and temperature scales in the interface that are different from the convective scales, and to evaluate the properties of organized structures of turbulence using conditionally averaged statistics.

2. EXPERIMENTAL APPARATUS AND PROCEDURE

2.1. *Test section*

The test section consisted of a rectangular chamber (150 cm × 148 cm) filled with water and insulated on its top and sides (Fig. 1). The conditions that were achieved by the test section were: (a) a high aspect ratio (width to height) with negligible effects of the lateral walls in generating mean flow circulations, (b) negligible heat losses through the top and side walls, (c) parallel and horizontal plates, (d) a constant mean heat flux through the lower plate.

The test section was formed by a 2.5 cm thick aluminum horizontal plate at the bottom, two insulated glass walls in the front and the back and insulated plexiglass side walls, and an insulating wooden upper boundary. Heat was supplied to the aluminum plate by means of nine electrical heating mats bonded to the bottom of the plate, and connected to a power controller. The standard deviation of the multipoint temperature measurements at the upper surfaces of the aluminum plate averaged 0.09°C. For a full input power of 6 kW at 40°C the overall heat loss across the test section walls was estimated to be 1% of the input power. However, at the lower operating input case, there existed a loss of 5% of the input power.

2.2. *Temperature measurement*

The mean temperature was measured using a Teflon coated alumel wire strung back and forth across a stainless steel ring. The wire had the following characteristics: length, 3200 mm; diameter, 0.0762 mm;

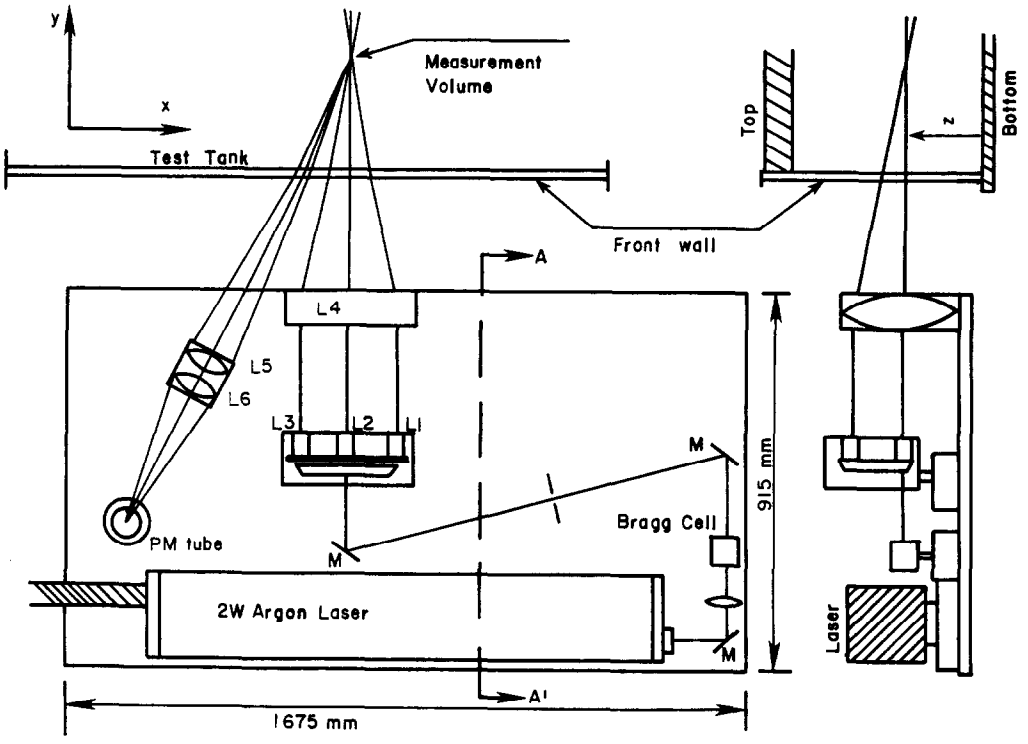

FIG. 1. Scanning table with optical components and the test section.

thickness of the insulation, 0.0762 mm; sensitivity, 0.370 Ω $°C^{-1}$. A bridge amplifier circuit was used to convert the resistance wire output to voltage. The combined probe and bridge amplifier sensitivity was 2.096°C V^{-1}, obtained by calibration. The vertical mean temperature profile was measured by scanning the resistance wire vertically from bottom to top at a speed of 0.478 cm s^{-1} giving a succession of temperature profiles as the experiment progressed. The time constant τ_w of the resistance wire was calibrated to be 240 ms. Details of the calibration procedure are given by Ferreira [22]. Fluctuating temperatures were measured by a thermocouple, constructed from chromel–constantan duplex wire which was spot-welded to form a measurement junction. The characteristics of the probe were: diameter, 0.0381 mm; stainless steel sheath diameter, 0.254 mm. The sensitivity of the thermocouple was estimated to be 60 μV $°C^{-1}$ within the operating range of 20–40°C. The time constant of the thermocouple was estimated to be 3.2 ms corresponding to a frequency of 50 Hz.

2.3. *LDV measurements and signal processing*

The horizontal and vertical components of the instantaneous velocity were measured with a two-component, dual-beam, laser-Doppler velocimeter operating in a back scatter mode. The system was arranged to form a 0.15 mm × 0.15 mm × 1.7 mm measurement volume located 2 mm on the left-hand side of the thermocouple to reduce probe interference with velocity (Fig. 1). The light source used was a 2 W argon ion laser. The two components of velocity were measured using a three-beam configuration as reported by Adrian [23].

The light scattered from the Dow Saran microsphere particles (diameter of 5–8 μm and specific gravity of 1.07) was collected in the off-axis backscatter mode (30° with respect to the y-axis shown in Fig. 1) by a photomultiplier tube. More details of the optical system, signal and digital processing are given in ref. [24]. The optical components and a support for the thermocouple were rigidly connected to an optical table which was mounted on a lathe bed and driven by a hydraulic piston along a horizontal path parallel to the bottom of the test section.

2.4. *Generation of a linear temperature gradient*

A linear temperature gradient was set up in the test section before the penetrative convection experiment began. Since the flow had to be seeded before setting up the temperature gradient, it was important that the linear profile was set up in less than 1 h so that the LDV measurements could be made for at least 2 h. Experiments could not be performed for longer periods since the scattering particles settled down denying a good velocity signal. A heating wire was wound around a horizontal aluminum frame as described in ref. [24]. This frame was arranged in such a way that it could be cranked upwards inside the water layer and fixed at specific heights. A stepwise temperature gradient was set up by moving the frame to different heights for time intervals calculated from the heat balance equation for the layer of water between the frame and the top of the convection chamber. The

resulting temperature steps are smoothed out by conduction to give a linear temperature profile. The above mentioned step method was found to be several times faster than the traditional method of adding warmer layers using wooden floats. Mean temperature measurements were made at different times, and the convection and stable regions were linear fitted, and the intersection of these two lines was defined as the height of the interface. These experimentally determined interfacial growth rate profiles were given in ref. [6] and were found to agree very well with the zero-order model of Deardorff *et al.* [25].

2.5. *Noise due to refractive index fluctuation*

In most practical situations, signals are degraded to an extent by background noise. The main source of noise in the present flow situation was due to the random fluctuations of refractive index of the medium. In the region of measurements in the interfacial layer, the intense temperature fluctuations gave rise to refractive index fluctuations. Hence, the laser beam would propagate with randomly fluctuating curvature causing distortion and misalignment. In order to reduce this type of noise which was a maximum where σ_θ was a maximum and decreased away from this narrow region, the optical table was tilted by 2° so that only a portion of the laser beam would have to go through the region of maximum refractive index fluctuations. To evaluate the magnitude of the noise added to the velocity signal by refractive index fluctuations, a stationary plexiglass target was placed in the water tank after the stable layer was set up. The scratches on the surface of the target behaved as stationary scattering particles that had zero velocity. Fluctuations in the resulting velocity measurements then corresponded to refractive index noise fluctuations. The mean square noise only due to refractive index fluctuations was evaluated by subtracting the mean square noise (with no convection) from the total mean square noise. Under the worst case conditions, i.e. at $z = z_*$ where the temperature fluctuation is a maximum (as will be shown later), the r.m.s. noise was found to be maximum at $0.1w_*$, where w_* was the velocity scale of the convection layer. Away from the center of the interface, the noise due to refractive index fluctuations was small and buried in ambiguity noise. The signal quality decreased with increasing temperature gradient, Γ, and the bottom layer heat flux, Q_0. Hence, large Reynolds numbers and entrainment parameters were not achieved in the laboratory. For a high heat flux, $Q_0 = 0.024$°C cm^{-1} s^{-1} (Case D), velocity could not be measured for $\Gamma = 0.55$°C cm^{-1}. Hence, the parameters were chosen such that refractive index noise could be contained. Measurements of $\overline{w\theta}$, $\overline{w\theta^2}$, and $\overline{w^2\theta}$ were not expected to be affected by refractive index noise if the noise did not correlate well with the local temperature fluctuations. Measurements of the r.m.s. velocity contained a component due to noise, however, the magnitude of this component is less than 5% of the total r.m.s. velocity in the region above $z/z_* = 1.0$.

2.6. *Data analysis*

Measurements were made by scanning the optical table in the middle third of the test section at a speed of 2.735 cm s^{-1}. Each scan consisted of 1024 points, with a digitization time interval of 0.0144 s between successive points and a Nyquist frequency of 35 Hz. Measurements were made at a fixed line allowing the interface to cross the measurement line. Hence, the aspect ratio, $A(=h/z_*)$ decreased from 15 for measurements at the top of the interface to 7.25 in the mixed layer. It was assumed that this aspect ratio range was high enough to trust that mean circulation did not affect the measurements. The other assumptions made about the flow situation were: (a) the flow was horizontally homogeneous and hence the mean quantities depended only on the vertical direction, (b) ensembles could be formed so that ensemble averages were equivalent to averages formed over horizontal lines, (c) the growth of the mixed layer was slow enough that a quasi-steady state existed for a short time period in which at least two scans of measurements were obtained. Hence, the turbulent moments were functions of the height, z, only.

Since the interface migrated upward with time, continuous measurement scans were made at a fixed height ($z = 13$ cm), letting the interface pass through the measurement line. The time of each scan and the interface height were noted. Collecting two scans of data from each experiment, 12 scans of data were grouped for one non-dimensionalized height. With reference to Fig. 1, velocity measurements were made scanning the table in the negative x-direction, i.e. from right to left, since the thermocouple probe was located to the right of the measurement volume. However, in the return scan, fluctuating temperature measurements were made. Hence, when only 12 scans of data were available for ensemble averaging σ_w, $\overline{w^2}$, $\overline{w^3}$, $\overline{w\theta}$, $\overline{w\theta^2}$, and $\overline{w^2\theta}$, 24 scans were available to analyze σ_θ, $\overline{\theta^2}$, and $\overline{\theta^3}$. The peak in σ_θ in each experiment formed the basis for grouping, and the height at which this peak occurred was tagged as the interface height, z_*. Thus, detailed measurements were made in the interfacial zone (nearly 25 points for each case within 4–4.5 cm). Some overlap occurred but any error caused by such an overlap was insignifcant. More details of the data collection procedure can be found elsewhere [24].

3. RESULTS AND DISCUSSION

3.1. *Turbulence scales in the entrainment zone*

In the experiments which involve a linear temperature gradient above a turbulent mixed layer, the temperature jump in the interface is not well defined since the interface is not well defined. In the entrainment zone of penetrative convection, z_* is defined as the height at which temperature fluctuations reach a

maximum. Reference [6] presented higher order moments in the entrainment zone. In that work, traditional convective scales were used and σ_θ data were not well correlated above $z/z_* = 1$ and σ_θ appeared to be affected by the temperature gradient, Γ, in the stable layer. The entrainment zone is conveniently defined as the layer (Δh) where the mean buoyancy flux is negative. This thickness of the entrainment zone, Δh, at which $\overline{w\theta}$ is negative, was seen to decrease with increasing stratification. These observations suggest that the interface needs to be characterized by interfacial temperature and length scales.

If ΔT is the maximum negative temperature a penetrating parcel experiences at the interface, and Δh is the distance the parcel penetrates, the maximum restoring buoyancy force becomes proportional to $\beta g \Delta T$. If a force balance is written between the inertial force and the restoring buoyancy force (ignoring dissipation), and integrated across the entrainment zone, one can write

$$\frac{w_*^2}{2} \propto \beta g \, \Delta T \, \Delta h \tag{5}$$

where w_*, the convective velocity scale, is proportional to the velocity entering the interface. If the turbulence time scale in the interfacial layer is assumed to be proportional to the Brunt–Väisälä period

$$t_{BV} = \frac{1}{\sqrt{\left(\beta g \dfrac{\Delta T}{\Delta h}\right)}} \tag{6}$$

then

$$\Delta h \propto \frac{w_*}{\sqrt{\left(\beta g \dfrac{\Delta T}{\Delta h}\right)}} \propto \frac{w_*}{\sqrt{(\beta g \Gamma)}} \tag{7}$$

and

$$\Delta T \propto \Gamma \, \Delta h = \sqrt{\left(\frac{\Gamma}{\beta g}\right)} w_*. \tag{8}$$

Hence, the turbulence scales used to collapse the data are

$$l = \frac{w_*}{\sqrt{(\beta g \Gamma)}} \propto \Delta h$$

$$\theta_c = \Gamma l \propto \Delta T \tag{9}$$

and

$$w_* = (\beta g Q_0 z_*)^{1/3}$$

where Q_0 is the kinematic heat flux at the bottom plate. Thus, the entrainment zone is characterized by both its thickness and temperature discontinuity. A similar length scale based on interfacial distortion was proposed by Wyatt [9].

Selected samples of fluctuating temperature are given in Fig. 2 from representative experiments of Case C. Measurements have been made at different non-dimensionalized heights, $z' = (z - z_*)/l$. Figure 2(a) represents a data scan in the non-turbulent stable layer, Fig. 2(c) represents a data scan close to the middle of the interface where σ_θ is a maximum, and Fig. 2(f) represents a data scan in the mixed layer. Townsend [4] proposed that the large temperature fluctuations found in the stable region are due to internal gravity waves which are caused by impacts of ascending fluid columns. From Fig. 2(a) and representative data from other experiments of Case C, the period of internal gravity waves is seen to be close to 7 s. This is somewhat smaller than the Brunt–Väisälä period of 11.4 s for Case C (Table 1). However, they are of the same order of magnitude, suggesting that the turbulence time scale in the entrainment zone is proportional to the Brunt–Väisälä period as was originally assumed. Longer periods may be expected deep in the stable region. Temperature fluctuations become large in the middle of the interface as seen in Figs. 2(c) and (d). In this region, the period becomes smaller as the middle of the interface reaches the probe. As the interface migrates upwards away from the probe. As the interface migrates upwards away from the probe, fluctuations become relatively small, with the r.m.s. value close to the convective temperature scale, $\theta_*[\theta_* = Q_0/w_*]$.

Profiles of the mean temperature (T vs z) were first plotted at different times. Noting the interfacial height, z_*, at different times, these profiles were replotted as $(T - T_\infty)$ vs $(z - z_*)/l$. Some representative temperature profiles at the beginning and end of an experiment for Cases A–D are given in Fig. 3. Analyzing many such plots for each of the four cases, it can be confidently reported that the profiles are nearly self-similar, and the linear temperature gradient above the interface was maintained for the most part of an experiment.

In Case D, the interfacial cooling appears to be more pronounced as the mixed layer grows upwards. This interfacial cooling phenomenon has been reported by a number of investigators and it causes the entrainment region to be more stable than the non-turbulent stable region atop. The thermal overshoot depends upon the temperature gradient in the stable layer and the heat flux at the bottom plate. Although there is interfacial cooling in Cases B and C, the thermal overshoot does not appear to be significant in the corresponding temperature profiles.

3.2. *Unconditionally averaged moments*

All the moments nondimensionalized using the interfacial scales are presented in Figs. 4–8. A solid line is sketched through the data in some figures to indicate what is believed to be the general trend. The r.m.s. values of the horizontal component of velocity, σ_u, the vertical component, σ_w, are given in Fig. 4. The thermals that do not have an entirely vertical motion penetrate up to $(z - z_*)/l = z' \simeq 3.0$ decelerating as they traverse the entrainment zone. Both σ_u and σ_w

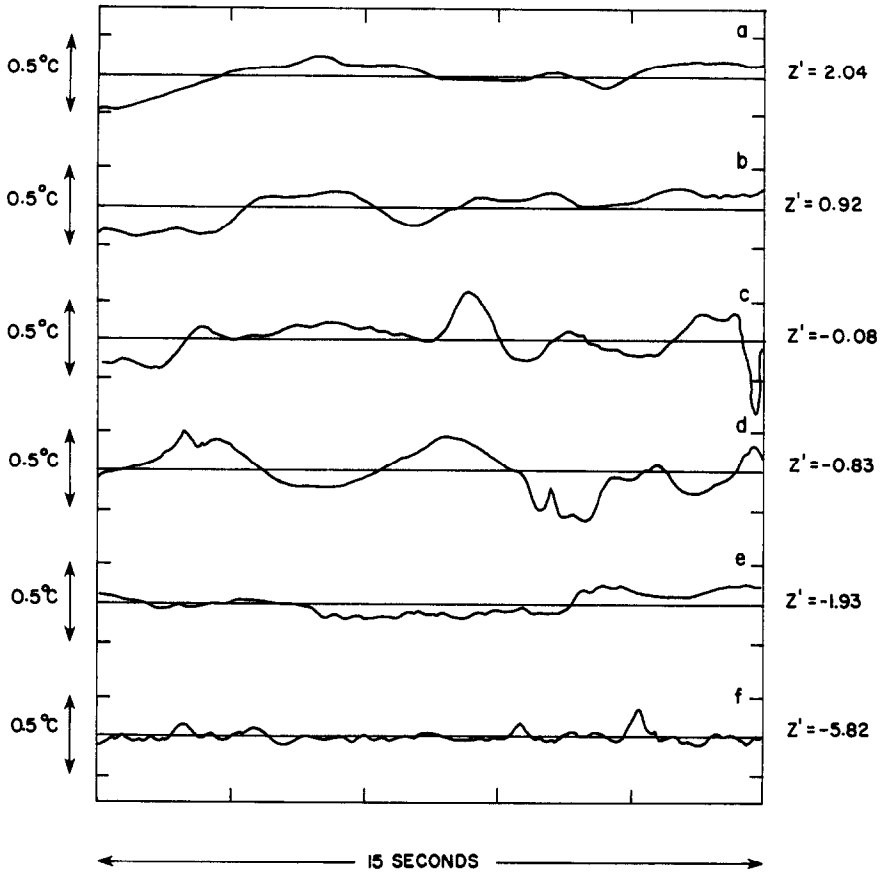

FIG. 2. Records of fluctuating temperature for Case C. Non-dimensionalized heights are given on the right.

profiles exhibit comparable motions at $z' = 0$ associated with ascending thermals spreading to the sides due to impacts. It is to be noted that at $z' = 0$, $\sigma_u = \sigma_w \simeq 0.2w_*$, and the r.m.s. noise due to the refractive index at this same level is estimated to be $0.1w_*$. However, the r.m.s. refractive index noise falls off rapidly away from $z' = 0$.

The temperature scale, θ_c, seems to collapse the r.m.s. temperature fluctuation data much better than θ_*, as shown in Fig. 5. The temperature and length scales for the different cases are given in Table 1. At $z' = 0$, σ_θ attains a sharp peak with a value of $0.3\theta_c$. The ascending hot fluid elements from the bottom plate turn relatively cold when they enter the entrainment zone, and on average penetrate up to $z' = 0$. Although at $z' = 3.0$, the r.m.s. velocities die out, the r.m.s. temperature reaches a near constant value of $0.15\theta_c$. Deardorff and Willis [26] extended their experimental results of penetrative convection in a water tank and presented turbulence intensities, spectra and probability distributions. Their five experimental points in the region of interest replotted using the interfacial scales given in equation (9) compare well with the present data (Figs. 5 and 6).

The presence of interfacial cooling is clearly seen from the heat flux profile in Fig. 6. The magnitude of the negative heat flux is a fraction of the input heat flux at the bottom plate. Whether or not this fraction depends on the stability gradient cannot be inferred easily from the present data, since the scatter in the cross-correlation is quite high. However, the extent of the region between zero crossings of the heat flux

Table 1

Case	Symbol	$\Gamma = \frac{dT}{dz}$ (°C cm^{-1})	Q_0 (°C cm s^{-1})	z_* (cm)	w_* (cm s^{-1})	θ_c (°C)	$Re_* = w_* z_*/\nu$	ω_B (rad s^{-1})	$l = w_*/\sqrt{(\beta g \Gamma)}$ (cm)	$\frac{dz_*/dt}{w_*}$
A	△	0.29	0.0133	13	0.371	0.368	560	0.292	1.27	0.0109
B	⊙	0.55	0.0133	13	0.371	0.507	560	0.402	0.922	0.0056
C	★	1.026	0.0133	13	0.371	0.693	560	0.55	0.675	0.0025
D	□	0.55	0.0241	17	0.494	0.675	975	0.402	1.228	0.0049

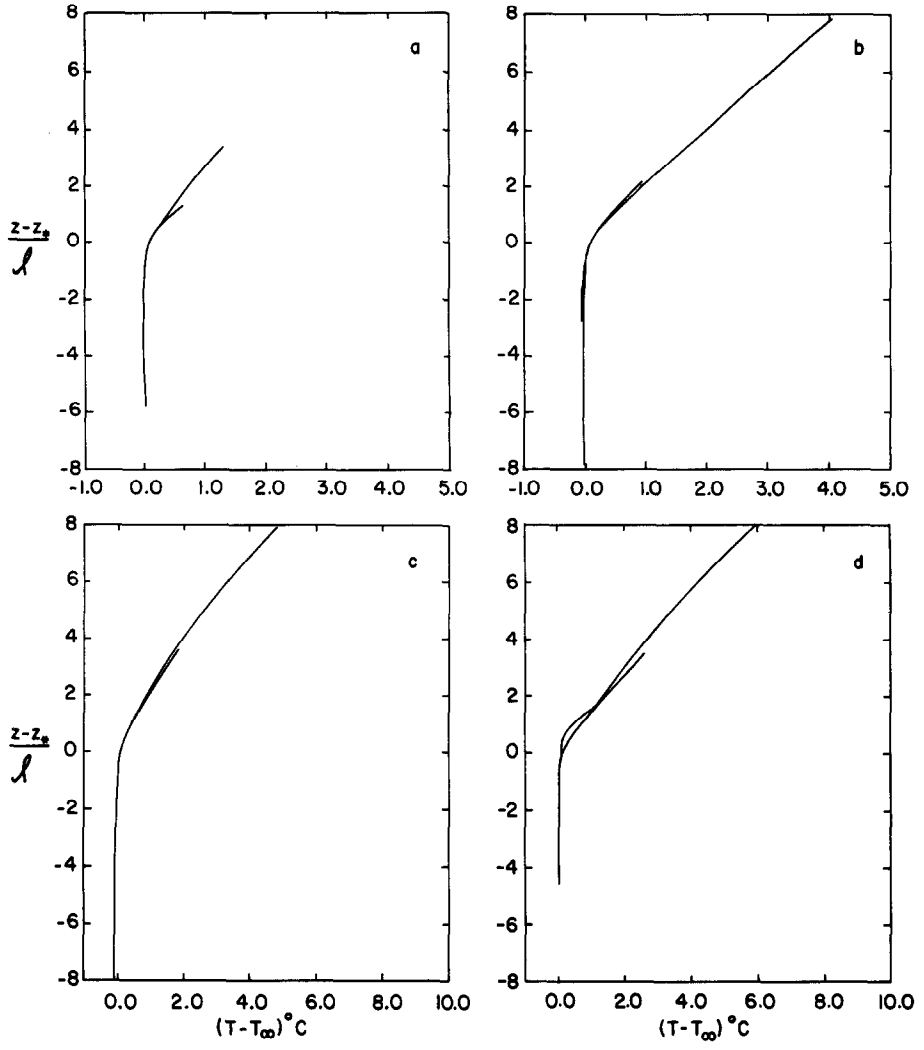

FIG. 3. Mean temperature profiles (from one experiment) at the beginning (----) and end (----) of the experiment for: (a) Case A; (b) Case B; (c) Case C; (d) Case D.

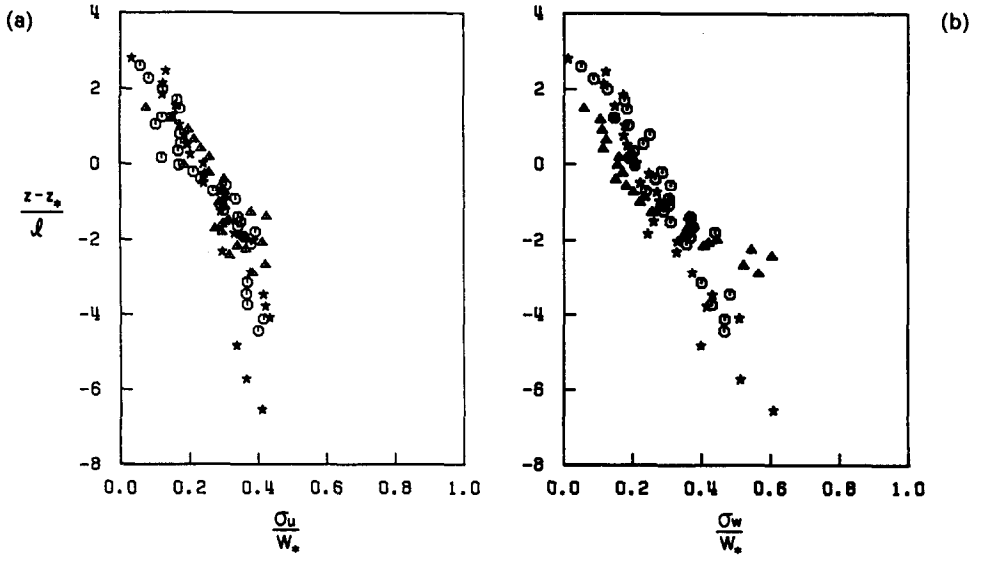

FIG. 4. (a) Root-mean-square horizontal velocity fluctuations. (b) Root-mean-square vertical velocity fluctuations. Δ, Case A; ⊙, Case B; ★, Case C.

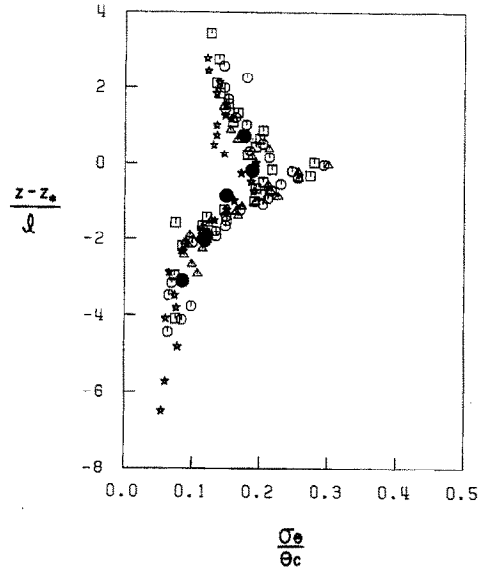

FIG. 5. Root-mean-square temperature fluctuations. Δ, Case A; ⊙, Case B; ★, Case C; □, Case D; ●. Deardorff and Willis [26].

profile in each case seems to confirm the presence of a length scale which is dependent upon the interfacial thickness. The reason for the negative heat flux to be small in magnitude for Case A may be attributed to experimental error in the entrainment zone. For all three cases, the negative heat flux region extends from $z' = 0.5$ to -2.5 indicating that the interfacial thickness is approximately equal to $3.0l$. On average, most negative heat flux occurs l cm below $z' = 0$, where l is the length scale in the interfacial layer. Above $z' = 0.5$, the data exhibit a small positive region in all three cases. The heat flux becomes positive below $x' \simeq -2.5$.

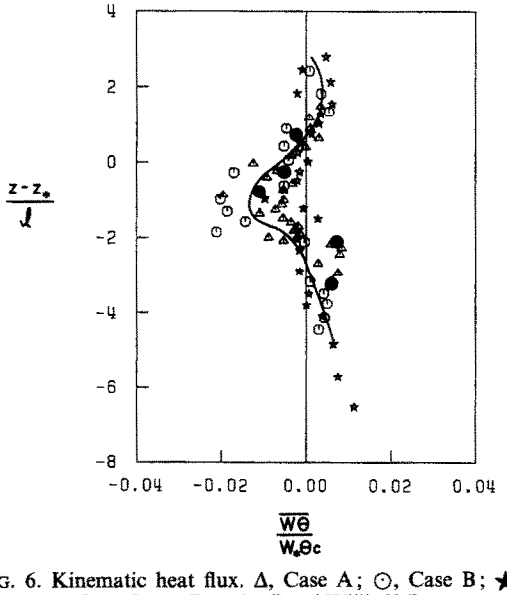

FIG. 6. Kinematic heat flux. Δ, Case A; ⊙, Case B; ★, Case C; ●, Deardorff and Willis [26].

A complete picture of the dynamical processes near the interface may be obtained by examining the vertical profiles of third-order moments. The measurements of $\overline{\theta^3}$, $\overline{w\theta^2}$, $\overline{w^2\theta}$, and $\overline{w^3}$ are useful because their signs reveal the direction of the velocity and the relative temperature of the thermals in that region. Although sampling errors in the third-order moments are large, some of the scatter is contained if the proper scaling is used. Also, the third-order moments exhibit the same sort of variations in all the cases. Hence, qualitatively these moments can be treated with confidence.

Figure 7(a) shows a sharp negative peak at $z' = 0$ in the $\overline{\theta^3}$ profile. In the region between $z' \simeq 0.5$ and -1, the penetrating thermals with large negative fluctuations contribute to the negative $\overline{\theta^3}$. This is consistent with the $\overline{w\theta^2}$ profile in Fig. 7(b). In the same region where $\overline{\theta^3}$ is negative, $\overline{w\theta^2}$ is positive meaning that the ascending thermals with w and $-\theta$ contribute the most in this region. Figures 8(a) and (b) show similar trends in $\overline{w^3}$ and $\overline{w^2\theta}$ in this region.

In the tiny region near $z' = 0.5$, $\overline{\theta^3}$ and $\overline{w^2\theta}$ profiles (Figs. 7(a) and 8(b)) show a slight positive region. If the positive values of θ are due to entrainment, $\overline{w\theta^2}$ and $\overline{w^3}$ (Figs. 7(b) and 8(a)) must show negative values in this region. The diffusion of kinetic energy in this region is nearly zero, making the pressure diffusion the only source to maintain the turbulence against losses due to viscous dissipation and negative buoyant flux. The turbulent diffusion of the temperature variance, $\overline{w\theta^2}$ in Fig. 7(b) shows slight regions of both positive and negative values. It is not expected that most thermals could have penetrated up to $z' \simeq 2.0$. However, the intermittency in turbulence probably makes this region convoluted obscuring horizontal homogeneity. This could have led to the weakly positive values of $\overline{w\theta^2}$.

At $z' = -1$, Fig. 7(a) shows both positive and negative values of $\overline{\theta^3}$ meaning that the rising and falling fluid elements contribute equally. This fact is substantiated by Fig. 7(b) at the same non-dimensionalized height, $z' = -1$, where $\overline{w\theta^2}$ is nearly zero. The downward entraining warm fluid and the upward penetrating cold fluid contribute in such a way that their opposing statistical characteristics cancel out. It is interesting to note that it is at this height $z' = -1$ that the heat flux is most negative. The $\overline{w^2\theta}$ profile, however, stays predominantly negative in this region.

Below $z' = -2.5$, $\overline{w\theta^2}$ and $\overline{\theta^3}$ reach a small positive value. The fluid is positively buoyant in this region. The diffusion of kinetic energy becomes nonzero close to $z' \simeq -2$, increases slowly towards the core of the mixed layer, where the net diffusion vanishes as seen by Adrian [5] and Ferreira [22]. In general, below $z' = -2.5$, small positive temperature fluctuations and large positive velocity fluctuations dominate, indicating penetration is the only mechanism describing the structure of turbulence. Consequently, the convective scales should collapse the data better below $z' = -2.5$ as shown in ref. [6].

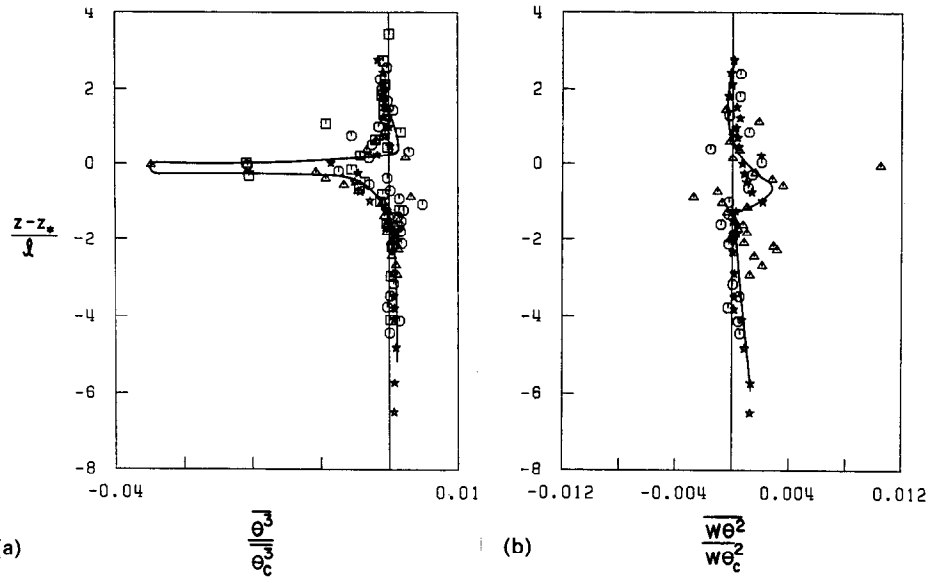

FIG. 7. (a) Third-order moment of temperature fluctuations. (b) Turbulent diffusion of the temperature variance. Δ, Case A; ⊙, Case B; ★, Case C; □, Case D.

The dominance of various mechanisms competing in the interfacial layer may be inferred by the sequence of probability density distributions for temperature fluctuations given in Figs. 9 and 10 for Cases B and C, respectively. Above $z' = 0.5$ in both Cases B and C, the positive fluctuations occur with sufficient frequency to result in net positive skewness. Figures 9(b) and 10(c) show that near $z' = 0$, the frequency of penetrating thermals (extending to nearly $-0.8\theta_c$) is slightly higher than the frequency of the entraining thermals (extending up to 0.7). This is the region where σ_θ and $\overline{\theta^3}$ exhibit a sharp peak. Figures 9(d) and (e) show bimodal lobes of temperature distributions, meaning that there may be two mechanisms present. This behavior is also supported by the third-order moments, particularly $\overline{w\theta^2}$, which vanishes near $z' = -1$ (Fig. 7(b)). In Case C, the stable temperature gradient is larger and hence fewer thermals penetrate up to $z' \simeq 0$. Consequently, the frequency of warm thermals entraining downwards is also less. This is why a positive side lobe is absent for Case C near $z' = -1$ (Fig. 10(d)). In the lower part of the interfacial layer (Figs. 9(f) and 10(f)), small temperature fluctuations occur. This fact is also supported by the raw temperature data in Fig. 2(f). Closer to $z' \simeq = -1.5$, both positive and negative fluctuations of temperature are probable as seen from the normal distributions centered around $\theta = 0$. Near $z' \simeq -4$, temperature fluctuations are expected to be positively skewed, characterizing thermals penetrating from the

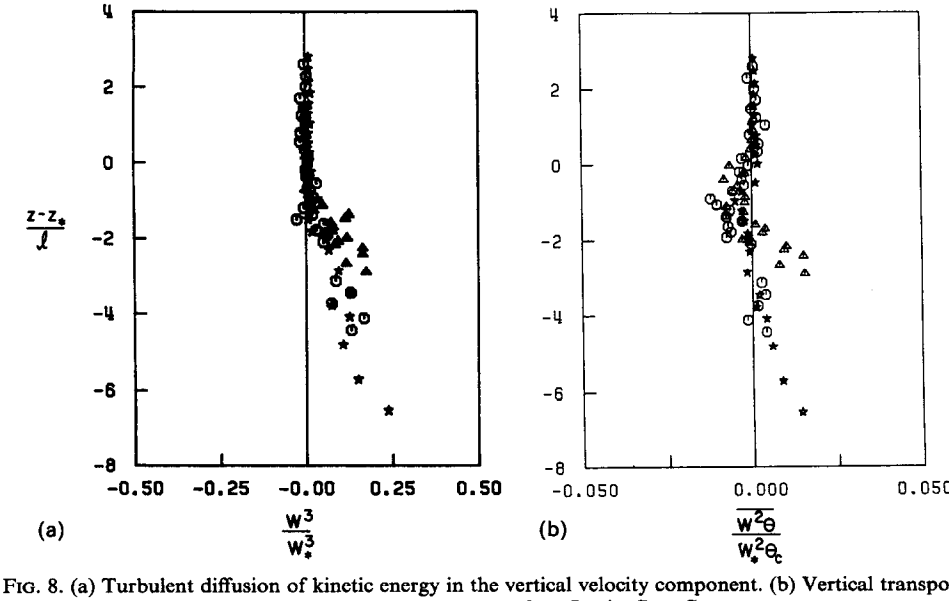

FIG. 8. (a) Turbulent diffusion of kinetic energy in the vertical velocity component. (b) Vertical transport of heat flux. Δ, Case A; ⊙, Case B; ★, Case C.

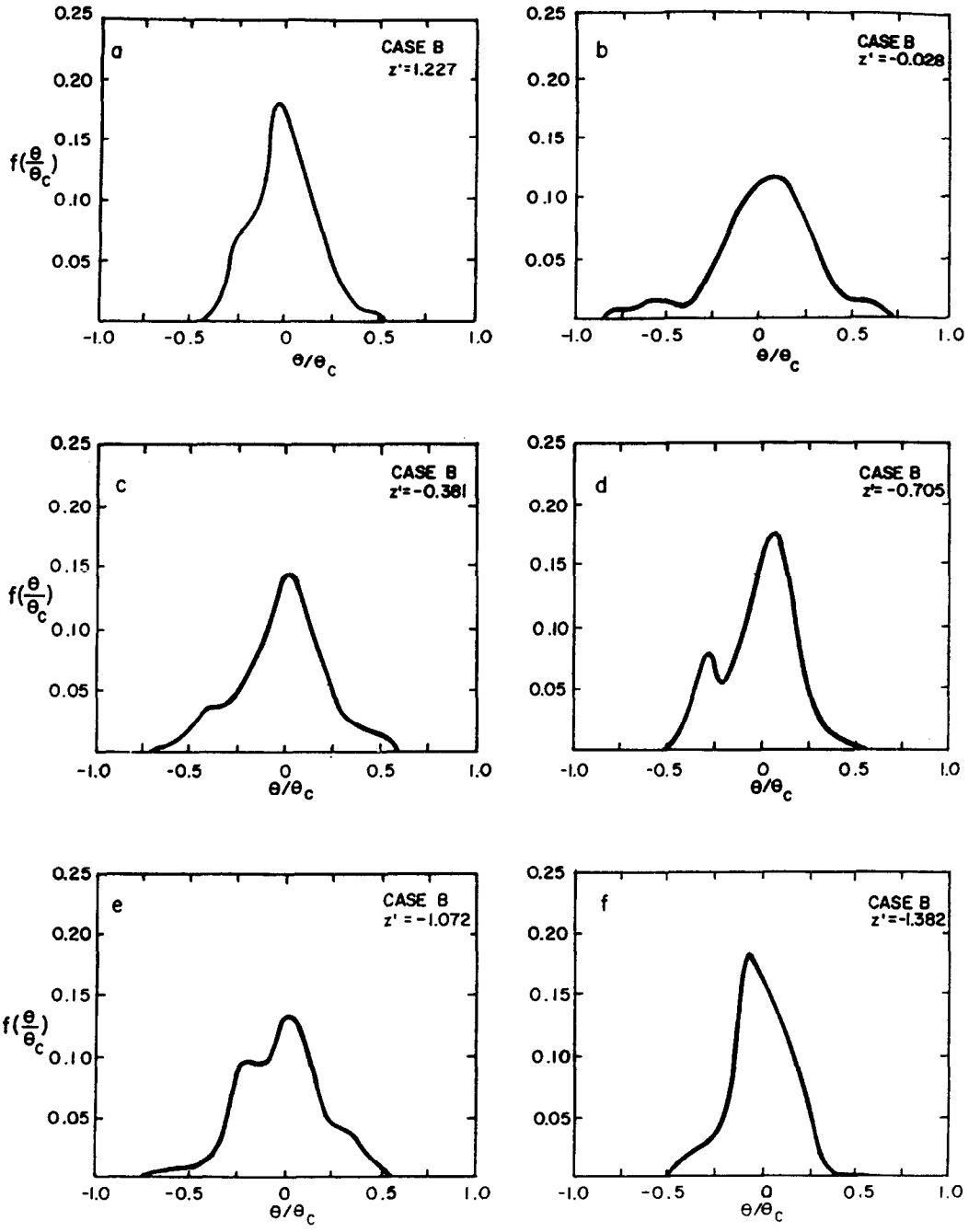

FIGS. 9(a)–(f). Probability density distributions of temperature fluctuations in the interfacial region for Case B. The corresponding non-dimensionalized height is given inside each figure.

bottom plate. Velocity distributions at different heights were seen to be nearly normal in all the cases.

3.3. *Conditionally averaged moments*

In order to determine the presence of organized structures in the flow field, the data have been conditionally averaged. Averaging the moments conditionally is essential to assess the properties of the thermals quantitatively. For convenience, the organized or 'coherent' structures are assumed to contain large velocity and temperature fluctuations the contributions to the heat flux of which have the same sign as the local unconditionally averaged heat flux. The idea of coherent fluid corresponds to the concept of 'active' fluid observed by Townsend [27] and Adrian [5] in their water-over-ice convection experiment. By this terminology, warm ascending fluid in the mixed

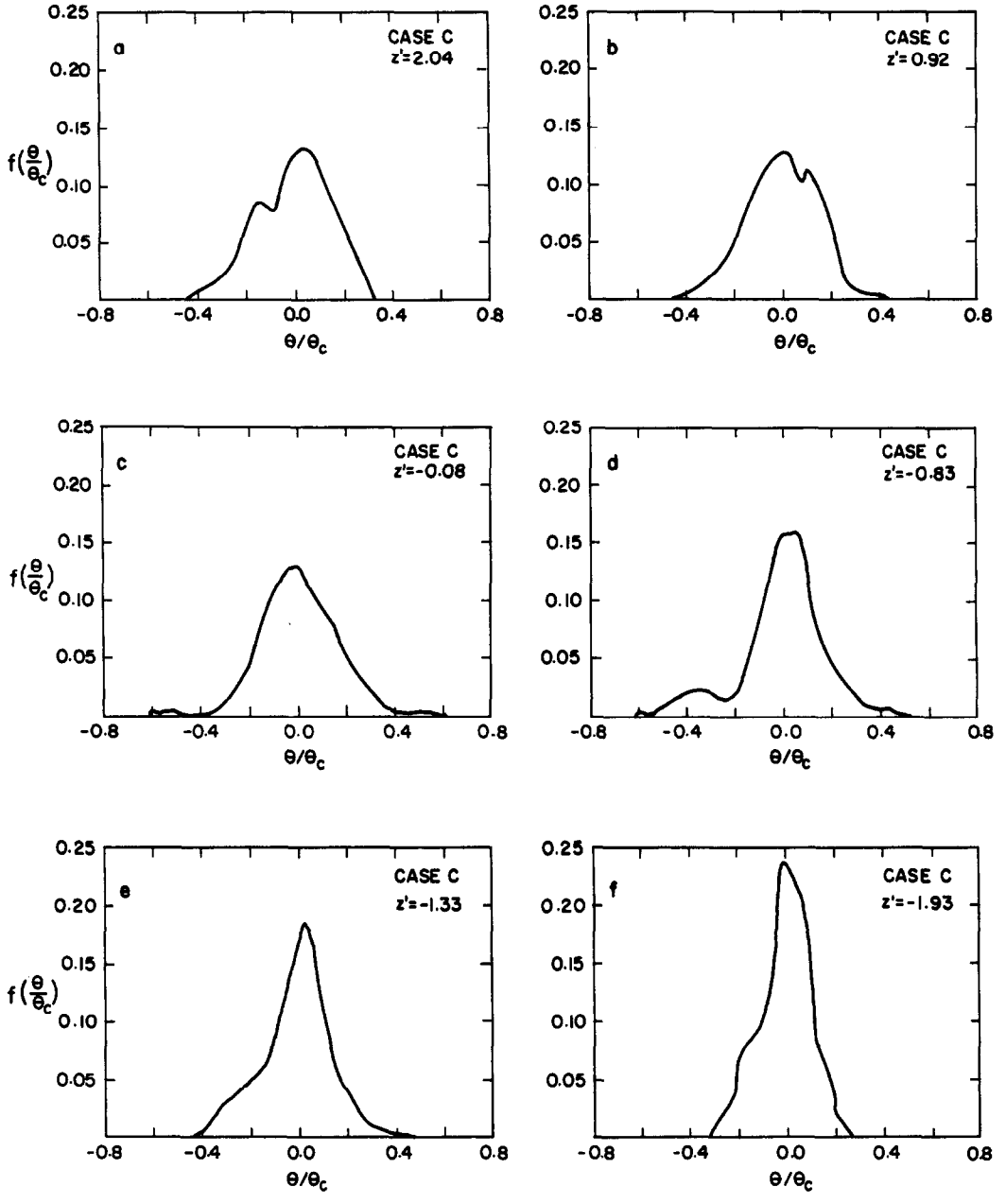

FIGS. 10(a)–(f). Probability density distributions of temperature fluctuations in the interfacial region for Case C. The corresponding non-dimensionalized height is given inside each figure.

layer turning relatively cold in the interface and the warm descending entrained fluid are active and could be termed coherent fluid. That is, active fluid elements are at a different temperature than that of the surroundings and are being acted upon primarily by buoyant forces. The 'inactive' or passive fluid, as the name indicates, is generally quiescent but is acted upon by the active fluid.

The data have been conditionally sampled based on a scheme followed by Adrian [5] to distinguish between coherent and incoherent fluid. The data points in the w–θ plane have been classified into five groups:

$$\begin{aligned} &\text{(I)} \quad w > 0, \theta > 0 \\ &\text{(II)} \quad w < 0, \theta > 0 \\ &\text{(III)} \quad w < 0, \theta < 0 \qquad |w\theta| > F\sigma_w\sigma_\theta \\ &\text{(IV)} \quad w > 0, \theta < 0 \\ &\text{(V)} \quad |w\theta| < F\sigma_w\sigma_\theta. \end{aligned} \tag{10}$$

In the interfacial layer where the heat flux is negative, groups II and IV correspond to coherent fluid and groups I and III correspond to incoherent fluid. Group V contains data points that do not fit in the first four groups with certainty. A discrimination level of $F = 0.1$ was set to categorize points in this group. This value was set with some compromise. Two

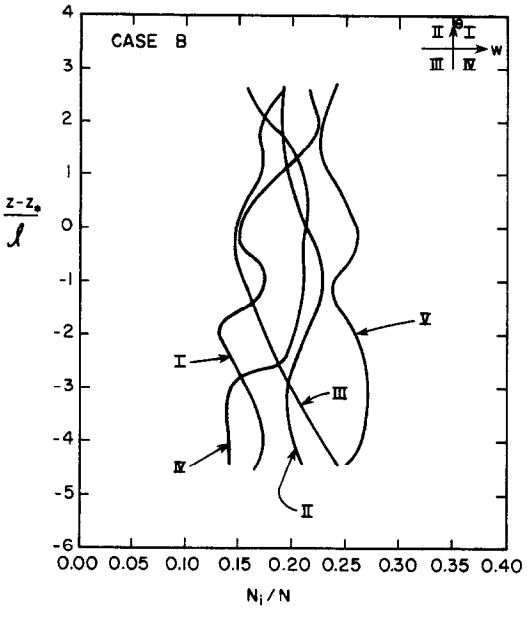

FIG. 11. Relative frequency of data points in groups I–V for Case B, $F = 0.1$.

types of conditional averages have been calculated. Given $G(w, \theta)$ as any function, $\overline{G_i}$ is the conditionally averaged mean of G belonging to the ith group

$$\overline{G_i} = \frac{1}{N_i} \sum_{a \in i} G(w_a, \theta_a), \quad i = \mathrm{I}, \ldots, \mathrm{V}. \tag{11}$$

The second type of average represents the fractional contribution made by the fluid belonging to a particular class to the total mean value of the quantity. The scatter in the conditionally sampled data was high. But, in general, similar trends were observed in both Cases B and C.

N_i/N represents the average horizontal area occupied by the fluid in the ith group. Profiles of conditionally averaged N_i/N for Case B are given in Fig. 11. The ascending warm fluid that belongs to group I is active as it traverses the mixed layer. But, as soon as it penetrates into the interfacial layer, the same fluid takes on negative temperature fluctuations and belongs to Group IV. This ascending coherent fluid extends from $z' = 1.5$ to -2.5 and occupies about 20% of the area. The majority of the entraining descending fluid in group II occupies the region $-2 < z' < 0$ and tapers off to nearly 20% above $z' > 2$. Inactive fluid $(-w, -\theta)$ of group III appears to be higher below $z' < -2$ where the thermals with $-\theta$ recede to lower levels of equal density. Similarly, inactive fluid of group I reaches its maximum above $z' > 1$ where the entraining fluid recedes to upper levels of equal density turning (θ, w). Group V occupies close to 25% of the total area reaching a maximum at $z' \simeq 0$ and again at $z' = -3$. A similar trend was observed by Adrian [5].

Conditionally averaged mean heat fluxes and their fractional contribution in the interfacial layer for Case B are shown in Fig. 12. The ascending coherent fluid of group IV dominates the region $-2.5 < z' < 0.5$, reaching a maximum value of nearly five times the total heat flux at $z' = -1$. The descending coherent fluid reaches a maximum of four times the total heat flux close to $z' \simeq 0$ and is seen to be dominant in the region $-1.5 < z' < 1$. Hence, the negative heat flux in the interfacial layer is predominantly due to the coherent fluid. The region of incoherent fluid peaking near $z' \simeq -0.5$ ranges between $z' = 0.5$ and -1.5. This means that the ascending fluid penetrates up to $z' = 0.5$ and some of the thermals recede due to mismatch of density, falling into group III. Most of these receding thermals reach only up to $z' = -0.5$. Similarly, some of the entraining fluid reach back to $z' = -1.5$ belonging to group I. The contribution from group V to the heat flux in negligible. From the unconditionally averaged moments, it was seen that $\overline{w\theta^2}$ was close to zero at $z' \simeq -1$ and $\overline{\theta^3}$ had both positive and negative values. It is now clear that such a behavior is due to the dominance of both penetrating and entraining mechanisms. Near $z' \simeq 0.5$, the slight hump that was seen in the $\overline{\theta^3}$ profile is now seen to be due to entrainment. Below $z' = -2.5$, group I dominates the heat flux. In this region, group I fluid is the ascending coherent fluid from the mixed layer that is associated with small positive temperature fluctuations.

Similar behavior is seen in Case C in Fig. 13. The ascending coherent fluid in the top of the mixed layer near $z' = -6$ (w, θ) is about five times the total heat flux at this point. Unlike in Case B, the relative maxima of incoherent fluid occur at different z'. The higher temperature gradient forces the penetrating thermals to bounce off deeper to create a hump closer to $z' = -1.5$ (group III). A similar situation occurs in the case of warm incoherent fluid (group I) which reaches a maximum near $z' \simeq 0$. However, the fractional contribution of the heat flux due to incoherent fluid stays nearly the same, occupying the region $-2.5 < z' < 0.5$. The contribution of the coherent and incoherent fluid seems to be nearly equal above $z' = -1.5$, however the small positive heat flux is due to incoherent fluid.

The fractional contribution of the variance of temperature fluctuation and variance of vertical velocity fluctuation for Case B are given in Figs. 14(a) and (b), respectively. On average, in the region, $-2.5 < z' < 1$, the coherent fluid occupies an area of 60% contributing to the variance of temperature and vertical velocity. The hump in the $N_i\overline{\theta_i^2}/N\overline{\theta^2}$ in group IV near $z' = 1.5$ may be spurious, but the contribution from all the groups except group V seem to be about equal above $z' = 1.0$. Comparing Figs. 11 and 14, it is interesting to note that the ascending coherent fluid belonging to group I (w, θ) changes sign $(w, -\theta)$ and moves into group IV at $z' \simeq -2.5$ making it the lowest point of the interfacial layer. However, such a feature indicating the zero cross-over is not discernible in the upper part of the interface.

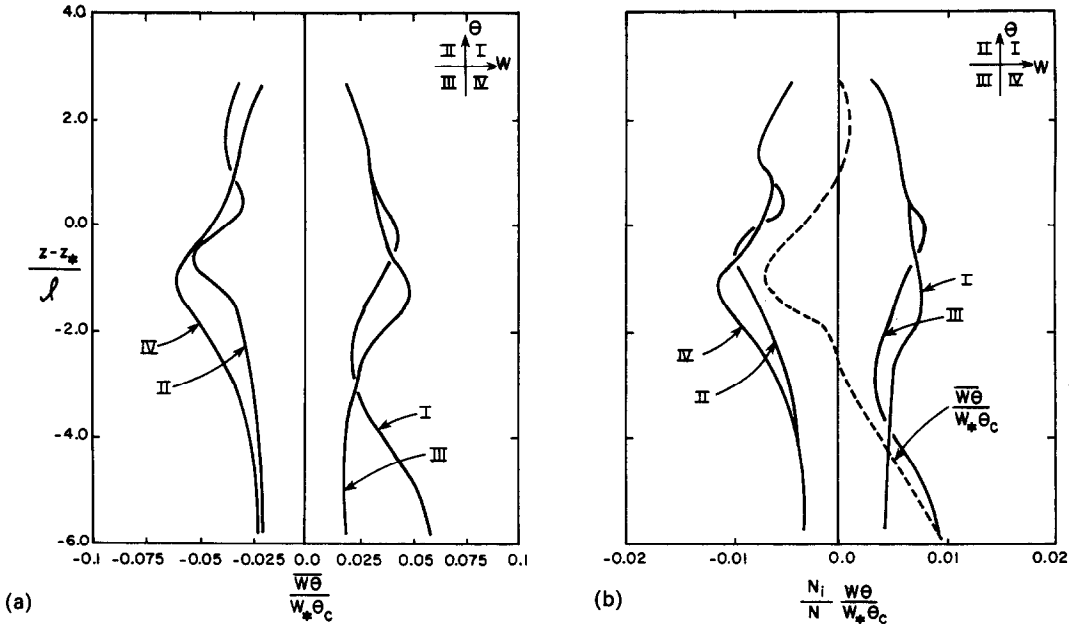

FIG. 12. (a) Conditionally averaged heat fluxes for Case B. (b) Fraction of the heat flux associated with groups I–IV for Case B, normalized by interfacial scales. ----, total heat flux normalized by interfacial scales.

4. SUMMARY AND CONCLUSIONS

Based on the horizontally-averaged single point moments, probability density distributions and conditionally-averaged statistics, the following conclusions may be drawn.

The turbulence time scale in the entrainment zone is seen to be proportional to the Brunt–Väisälä period. This leads to different length and temperature scales in the interfacial layer. The data collapse well for these turbulence scales, although these scales are derived for a non-mixing parcel of constant temperature.

The structured regions have been named 'coherent' and the coherent fluid dominates the interface; however, as the stability gradient is increased, there is less entrainment region corresponding to descending coherent fluid. The rising coherent fluid originates from the bottom plate near the conduction layer. In the mixed layer, the convective element accelerates with a velocity that exceeds that of the interface. When

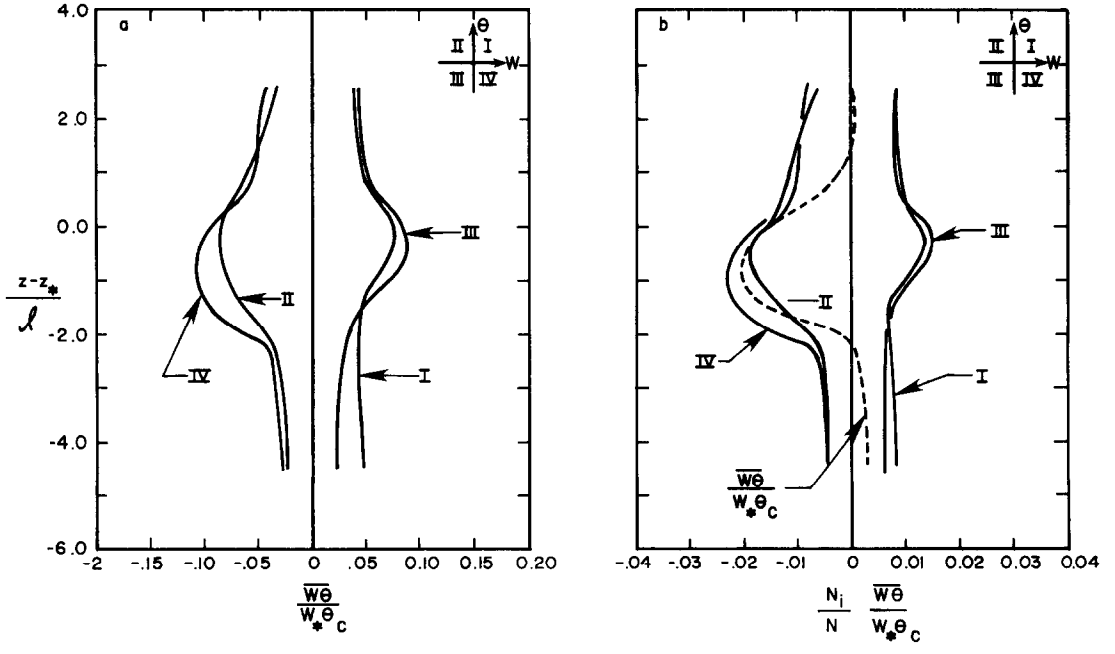

FIG. 13. Same as Fig. 12, but for Case C.

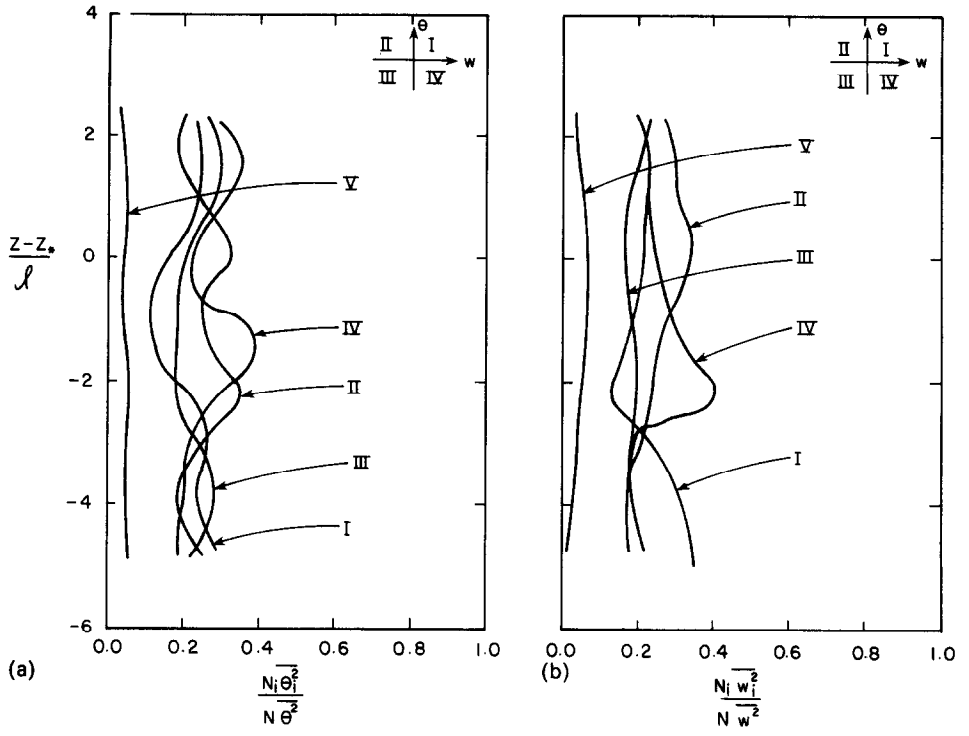

FIG. 14. (a) Fraction of the variance of the temperature fluctuation associated with groups I–V for Case B. (b) Fraction of the variance of the vertical velocity fluctuation associated with groups I–V for Case B. $F = 0.1$.

the fluid reaches the region of equal density, it decelerates but still penetrates above $z' > -2.5$ contributing to negative fluctuations of temperature. Thus, the same fluid contributes to two mechanisms: one takes the form of large, intermittent, positive velocity fluctuations associated with small negative temperature fluctuations; the other contributes to large temperature fluctuations and small positive velocity fluctuations. As a consequence of penetration, warm fluid from the stable region is entrained downwards to conserve mass. Thus, the negative heat flux is primarily due to both ascending and descending coherent (active) fluid, although conditional averages show that $(w, -\theta)$ contributes more than $(-w, \theta)$. Entrainment seems to play a dominant role in the region $0 \lesssim z' \lesssim 1$.

At $z' \gtrsim 1$, conditional averages show that all groups tend to be equal, probably indicating the presence of internal gravity waves with uncorrelated velocity and temperature fluctuations. Such an occurrence was also reported by Adrian [5] in his water-over-ice experiment. This region is convoluted by penetrating domes and subsiding thermals due to the restoring force of buoyancy obscuring horizontal homogeneity. This horizontal homogeneity may well depend on the entrainment parameter $(1/w_*)(\mathrm{d}z_*/\mathrm{d}t)$.

The entrainment parameter, $(1/w_*)(\mathrm{d}z_*/\mathrm{d}t)$, achieved in the laboratory is slightly lower than that found in the atmosphere ($\gtrsim 0.018$) but is of the same order of magnitude. It seems entirely adequate to model the penetrative convection of the lower atmosphere neglecting the effects of entrainment in the mixed layer. Although the magnitude of Reynolds number in the present experiment is much smaller than in the atmosphere, it may be large enough for the laboratory flow to behave as though its Reynolds number is asymptotically infinite, a condition needed for dynamic similarity to the atmosphere.

Acknowledgements—The author wishes to extend his sincere appreciation to Dr R. J. Adrian for his guidance, suggestions and many useful comments during the course of this work. Part of this work was supported by the National Science Foundation under Grant No. ATM 8203521.

REFERENCES

1. G. E. Willis and J. W. Deardorff, A laboratory model of the unstable planetary boundary layer, *J. Atmos. Sci.* **31**, 1297–1307 (1974).
2. H. D. Heidt, Comparison of laboratory experiments on penetrative convection with measurements in nature. In *Heat Transfer and Turbulent Buoyant Convection* (Edited by I. N. Spalding and N. Afgan), pp. 199–210 (1977).
3. R. J. Adrian and R. T. D. S. Ferreira, Higher order moments in turbulent thermal convection, 2nd Int. Turbulence Symp., London (1979).
4. A. A. Townsend, Natural convection in water over an ice surface, *Q. J. R. Met. Soc.* **90**, 248–259 (1964).
5. R. J. Adrian, Turbulent convection in water over ice, *J. Fluid Mech.* **69**, 753–781 (1975).
6. R. Kumar and R. J. Adrian, Higher order moments in the entrainment zone of turbulent penetrative thermal convection, *J. Heat Transfer* **108**, 323–329 (1986).
7. L. H. Kantha, O. M. Phillips and R. S. Azad, On turbulent entrainment at a stable density interface, *J. Fluid Mech.* **69**, 753–768 (1977).

8. J. W. Deardorff, G. E. Willis and B. M. Stockton, Laboratory studies of the entrainment of a convectively mixed layer, *J. Fluid Mech.* **100,** 41–64 (1980).
9. L. R. Wyatt, The entrainment interface in a stratified fluid, *J. Fluid Mech.* **86,** 293–311 (1978).
10. P. F. Crapper and P. F. Linden, The structure of turbulent density interfaces, *J. Fluid Mech.* **65,** 45–63 (1974).
11. E. J. Hopfinger and J. A. Toly, Spatially decaying turbulence and its relation to mixing across density interfaces, *J. Fluid Mech.* **78,** 155–175 (1976).
12. D. H. Lenschow, Model of the height variation of the turbulence kinetic energy in the unstable planetary boundary layer, *J. Atmos. Sci.* **31,** 465–474 (1974).
13. J. C. Kaimal, J. C. Wyngaard, D. A. Haugen, O. R. Coté, Y. Izumi, S. J. Caughey and C. J. Readings, Turbulence structure in a convective boundary layer, *J. Atmos. Sci.* **33,** 2152–2169 (1976).
14. S. J. Caughey and S. G. Palmer, Some aspects of turbulence structure through the depth of the convective boundary layer, *Q. J. R. Met. Soc.* **105,** 811–827 (1979).
15. D. H. Lenschow, J. C. Wyngaard and W. L. Pennell, Mean field and second moment budgets in a baroclinic, convective boundary layer, *J. Atmos. Sci.* **37,** 1313–1326 (1980).
16. D. J. Carson, The development of a dry, inversion-capped convectively unstable boundary layer, *Q. J. R. Met. Soc.* **99,** 450–467 (1973).
17. A. K. Betts, Non-precipitating cumulus convection and its parameterization, *Q. J. R. Met. Soc.* **99,** 178–196 (1973).
18. R. B. Stull, Inversion rise model based on penetrative convection, *J. Atmos. Sci.* **30,** 1092–1099 (1973).
19. H. Tennekes, A model for the dynamics of the inversion above a convective boundary layer, *J. Atmos. Sci.* **30,** 558–567 (1973).
20. J. W. Deardorff, Prediction of convective mixed layer entrainment for realistic capping inversion structure, *J. Atmos. Sci.* **36,** 424–436 (1979).
21. O. Zeman and J. L. Lumley, Modeling buoyancy driven mixed layers, *J. Atmos. Sci.* **33,** 1974–1988 (1976).
22. R. T. D. S. Ferreira, Unsteady turbulent thermal convection, Ph.D. Thesis, University of Illinois at Urbana-Champaign (1978).
23. R. J. Adrian, A bi-polar two component laser velocimeter, *J. Phys. E: Scient. Instrum.* **4,** 723–726 (1975).
24. R. Kumar, Studies in unsteady penetrative thermal convection, Ph.D. Thesis, University of Illinois at Urbana-Champaign (1983).
25. J. W. Deardorff, G. E. Willis and D. K. Lilly, Laboratory investigation of non-steady penetrative convection, *J. Fluid Mech.* **35,** 7–31 (1969).
26. J. W. Deardorff and G. E. Willis, Further results from a laboratory model of the convective planetary boundary layer, *Boundary Layer Met.* **32,** 205–236 (1985).
27. A. A. Townsend, Temperature fluctuations over a heated horizontal surface, *J. Fluid Mech.* **2,** 473–492 (1959).

ETUDES DE LABORATOIRE POUR LA CONVECTION THERMIQUE DANS L'INTERFACE D'UNE COUCHE STABLE

Résumé—Dans une expérience de convection naturelle pénétrante, des mesures détaillées des valeurs instantanées et locales de température, de composantes verticale et horizontale de vitesse sont faites en utilisant un thermocouple et un vélocimètre laser-Doppler à deux composantes. Dans la couche stable, on observe des ondes de gravité internes et les fluctuations de température dans cette région oscillent à une fréquence proche de celle de Brunt–Väisälä. Des techniques de moyenne conditionnelles et des distributions de densité de probabilité sont employées pour déduire les propriétés moyennes des éléments fluides dans la couche interfaciale. Les régions structurées sont dites "cohérentes" ou "actives" et elles comptent pour 60 à 70% des moyennes quadratiques des fluctuations de température et de vitesse et pour le flux thermique négatif. Des échelles interfaciales sont développées qui rassemblent bien les données et qui conservent la dispersion des moments du troisième ordre à l'intérieur des limites.

LABORUNTERSUCHUNG DER THERMISCHEN KONVEKTION IN DER GRENZSCHICHT UNTERHALB EINER STABILEN SCHICHTUNG

Zusammenfassung—Das Eindringen einer thermischen Auftriebsströmung in ein stabil geschichtetes Fluid wurde experimentell untersucht. Die momentane örtliche Temperatur wurde mit einem Thermoelement, und die waagerechten und senkrechten Geschwindigkeitskomponenten in der Grenzschicht wurden mit Hilfe eines Zweistrahl-Laser-Doppler-Anemometers detailliert gemessen. In der stabilen Schicht wurden innere Schwerkraftwellen beobachtet, und die Temperatur in diesem Bereich schwankte fast mit Brunt–Väisälä-Frequenz. Bedingte Mittelwertbildung und Wahrscheinlichkeitsdichte-Verteilungen wurden verwendet, um die mittleren Stoffwerte der Fluidteilchen in der Grenzschicht zu erhalten. Die Bereiche werden als "zusammenhängend" oder "aktiv" bezeichnet, und die Bewegungen berücksichtigen 60–70% der mittleren quadratischen Schwankungen von Temperatur und Geschwindigkeit und das meiste des negativen Wärmestroms. Kennzahlen für die Grenzschicht wurden entwickelt, welche die Daten gut wiedergeben und die Streuung der Momente dritter Ordnung in Grenzen halten.

ЛАБОРАТОРНЫЕ ИССЛЕДОВАНИЯ ТЕПЛОВОЙ КОНВЕКЦИИ НА МЕЖФАЗНОЙ ГРАНИЦЕ ПОД УСТОЙЧИВЫМ СЛОЕМ

Аннотация—При проведении эксперимента по проникающей конвекции, вызванной подъемными силами, с помощью термопары и двухкомпонентного двухлучевого лазер-допплеровского измерителя скорости детально измерены локальные мгновенные значения температуры, вертикальной и горизонтальной компонент скорости в межфазном слое. В устойчивом слое наблюдаются внутренние гравитационные волны, обнаружено также, что колебания температуры в этой области происходят с частотой, близкой к частоте Брунта–Вайсала. Для нахождения средних характеристик элементов жидкости в межфазном слое используются методы условного усреднения. Структурированные области называются "когерентными" и "активными", и именно они вызывают от 60 до 70% среднеквадратичных флуктуаций температуры и скорости, а также большую часть отрицательного теплового опотока. Разработаны масштабы для межфазных границ, которые сокращают данные и предотвращают большой разброс моментов 3-го порядка.